Supplementary information

Well Hydration and Cell-biologic Performances of Superparamagnetic Calcium Phosphate Cement with Concentration-dependent Osteogenesis and Angiogenesis Induced by Ferric Iron

Jing Zhang[a], Haishan Shi[a], Jingqun Liu[a], Tao Yu[a,c], Zhonghua Shen[d], Jiandong Ye[a,b,*]

1 Materials and methods

1.1 X-ray diffraction and structural analysis by the Rietveld refinement method of Fe-PCCP powders

The phase compositions of the sintered Fe-PCCP powders were assessed by X-ray diffraction (XRD; X'Pert PRO, PANalytical, the Netherlands). Data were collected from 10 to 80 degrees of 2θ with a scan step of 0.016^{o} and time/step of 80s using CuKα radiation (λ = 1.5418 Å). The obtained diffraction patterns were matched with the JCPDS (Joint Committee on Powder Diffraction Standards) cards to confirm the components. The Rietveld refinement method was carried out in order to calculate the lattice parameters and cell volume on the basis of XRD patterns using the software package FullProf Suite.

1.2 Morphology, atomic contents, and particle size distribution of Fe-PCCP powders

The morphology of Fe-PCCP powders was observed using scanning electron microscope (SEM; Nova NanoSEM 430, FEI, USA) after powders were scattered on conductive adhesive tape and sprayed with gold twice. Relative contents of Ca, P, and Fe in partial area of Fe-PCCP powders were detected by the attached energy dispersive spectrometer (EDS). The atomic contents of Ca, P and Fe in the final powders of these five groups were determined by X-ray fluorescence (XRF; PANalytical AXIOS, the Netherlands). The particle size distribution of Fe-PCCP powders was detected using laser particle size analyzer (Malvern, MS2000, UK).

1.3 Cytoskeletal organization of mBMSCs on Fe-CPC disks

The cytoskeletal organization of mBMSCs seeded on Fe-CPC disks was observed via staining the F-actin of mBMSCs with Phalloidin-iFluor^{TM} 488 Conjugate (AAT Bioquest, NO.23115, USA), and the nuclei of cells were stained with DAPI (AAT Bioquest, NO.17507, USA) at the same time. Cells on disks were rinsed with PBS once, immobilized with 4% paraformaldehyde solution for 20 min and submerged in 0.1 vol.% Triton X-100 solution for 5 min. Afterward, cells were labeled with the F-actin staining kit for 1 h and then counterstained with DAPI for 5 min according to the protocols. Fluorescence images were captured using confocal laser scanning microscope (Leica, SP5, Germany).

1.4 Synthesis of OCP and Fe-OCP powders

Calcium acetate monohydrate ($Ca(CH_3COO)_2 \cdot H_2O$, 0.02 mol/L), ammonium

biphosphate ($NH_4H_2PO_4$, 0.015 mol/L) and ferric nitrate ($Fe(NO_3)_3 \cdot 9H_2O$, 0.001 mol/L) was dissolved in deionized water and heat-treated in electric-heated thermostatic water bath at 90°C for 2 hours under stirring condition. Subsequently, the precipitant was washed and centrifugally separated with deionized water and absolute ethyl alcohol for 3 times and one time respectively and then centrifugally separated. The solid concentrate produced by centrifugation was collected and oven dried at 80°C to get OCP and Fe-OCP powders. All of the chemical reagents used here were analytical pure and purchased from Sigma.

2 Results and discussion

2.1 Phase compositon and the Rietveld refinement of Fe-PCCP powders

XRD patterns (Fig. S1) show that HA with low crystallinity was the main phase of all the five groups (0Fe-PCCP, 1Fe-PCCP, 2Fe-PCCP, 5Fe-PCCP and 10Fe-PCCP powders) after matching with the JCPDS card (HA JCPDS NO. 00-009-432), and no secondary phase was found after the increase of Fe^{3+} content. Lattice parameters of Fe-PCCP listed in Table S1 were obtained by Rietveld refinement method. Obviously, there was an increase of *a* axis and decrease of *c* axis with increasing amount of Fe^{3+}, which coincided with the previous study reported by VS Chandra *et al*. [1]. The gradual changing of lattice parameters demonstrated that Ca^{2+} ions in HA unit cell had been partially substituted by Fe^{3+} ions. Lattice parameters of 1Fe-PCCP and 2Fe-PCCP were close to each other but changed a lot in 5Fe-PCCP and 10Fe-PCCP. It's just because the difference of Fe^{3+} content between two groups was low in the former and a little larger in the latter.

It is well known that the relative intensity of diffraction peaks of different crystal planes is related to crystal orientation. Fig. S1b shows noticeable difference in the relative intensity of diffraction peaks of (211) crystal face and (202) crystal face ($2\theta = 31.766^{o}$ and $2\theta = 34.063^{o}$ respectively). The relative peak intensities of (211) crystal face were 65.9%, 87.2%, 81.8%, 61.6%, 56.2% respectively with the decreasing of Fe^{3+} content, with the highest peak intensity considered as 100% corresponding to (202) crystal face. The difference of relative peak intensity of $2\theta = 31.766^{o}$ to $2\theta = 34.063^{o}$ indicated that the introduction of Fe^{3+} in different contents into PCCP had an effect on the growth of (211) crystal face.

2.2 Morphology and Fe^{3+} content of Fe-PCCP powders

Fe-PCCP powders were composed of crystalline calcium phosphate and amorphous calcium phosphate as shown in Fig. S2. As the increase of Fe^{3+} content in PCCP, the morphology of crystals in Fe-PCCP gradually changed. In the groups of 0Fe-PCCP, 2Fe-PCCP, 5Fe-PCCP and 10Fe-PCCP (Fig. S2a,c,d,e), the crystalline calcium phosphate was plate-like. Whereas, in the group of 1Fe-PCCP (Fig. S2b), hexagonal prisms were found to be the main morphology of crystals. The morphology change and orientation of HA crystals might be attributed to the alteration of crystal surface energy which was caused by Fe^{3+} substitution. EDS analysis of the crystals in 10Fe-PCCP powders gave a atomic content of Ca (4.43%), P (3.12%) and Fe (0.77%), and the atomic ratio of (Ca+Fe)/P was 1.67 which was in accordance with the Ca/P ratio of stoichiometric HA (Fig. S2f). Both the change of lattice parameters and the result of EDS analysis indicated the substitution of Ca^{2+} by Fe^{3+}.

The XRF analysis showed the atomic ratios of Fe/(Ca+Fe) in Fe-PCCP powders (Table S2). The atomic ratio of Fe/(Ca+Fe) in Fe-PCCP powders on the basis of XRF results approximated to the pre-determined values and a gathering phenomenon of Fe^{3+} in the crystal part of Fe-PCCP powders was observed in the present study. Values showed here for 0Fe-PCCP, 1Fe-PCCP, 2Fe-PCCP and 10Fe-PCCP are a little larger than the original determined molar ratio, which can be ascribed to the loss of Ca in the synthetic process. However, it's difficult to exactly determine the iron content in crystals and amorphous part of Fe-PCCP powders respectively.

As shown in Fig. S3, the medium diameters of Fe-containing PCCP powders were larger than that of 0Fe-PCCP powder. The medium diameters of 0Fe-PCCP, 1Fe-PCCP, 2Fe-PCCP, 5Fe-PCCP and 10Fe-PCCP were 28.899 μm, 63.192 μm, 59.001 μm, 53.738 μm, and 54.772 μm, respectively. During the synthesis process, trivalent Fe^{3+} in HA crystals had stronger chemical attraction for phosphate groups, and then the growth of crystals was promoted.

Reference

[1] Chandra VS, Baskar G, Suganthi RV, Elayaraja K, Joshy MIA, Beaula WS, et al. Blood Compatibility of Iron-Doped Nanosize Hydroxyapatite and Its Drug Release. ACS Appl Mater Interfaces 2012;4:1200-10.

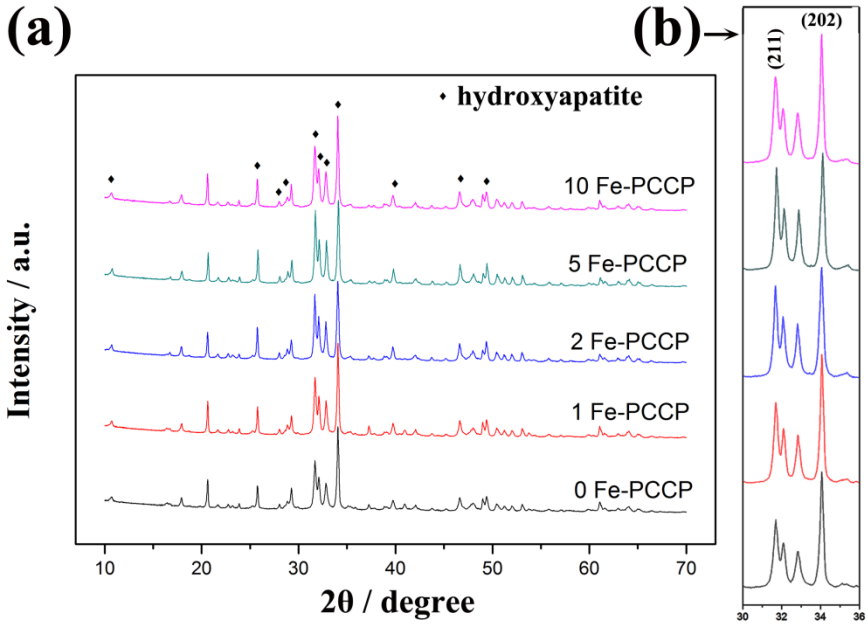

Figure S1. X-ray diffraction patterns (a) and magnified patterns from 30^{o}-36^{o} of 2θ (b) of synthesized PCCP and Fe-PCCP powders.

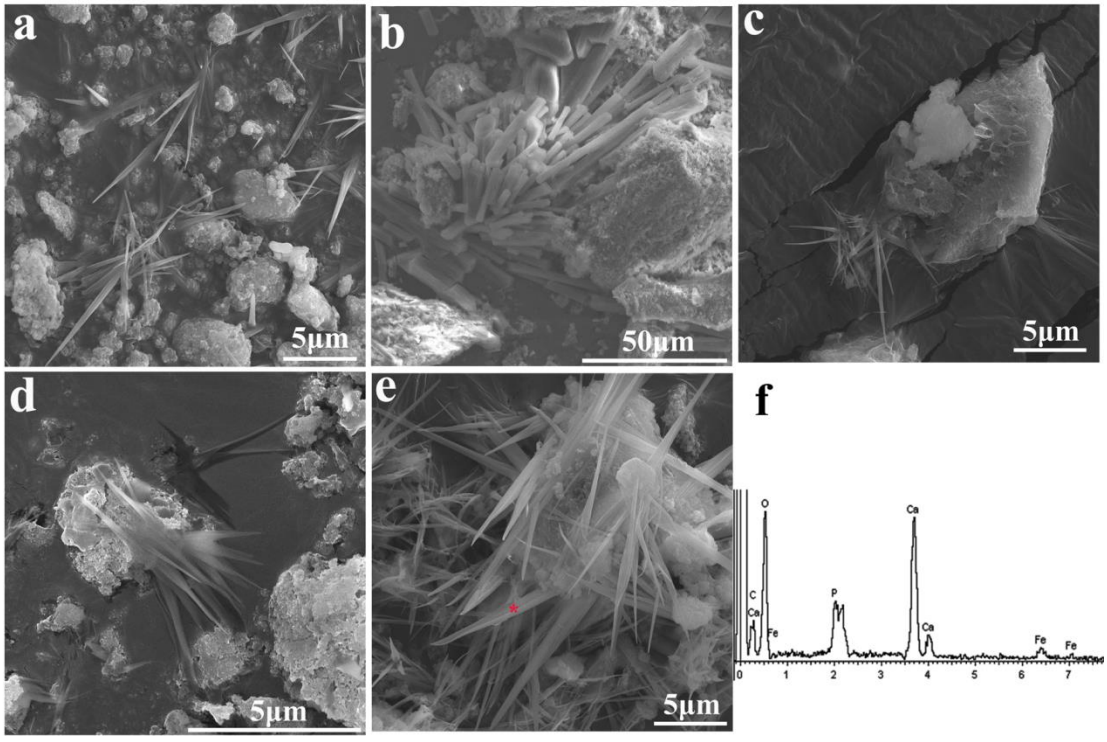

Figure S2. SEM images of 0Fe-PCCP (a), 1Fe-PCCP (b), 2Fe-PCCP (c), 5Fe-PCCP (d), 10Fe-PCCP (e), and EDS test result of the element composition of crystals (red * in image *e*) in 10Fe-PCCP (f).

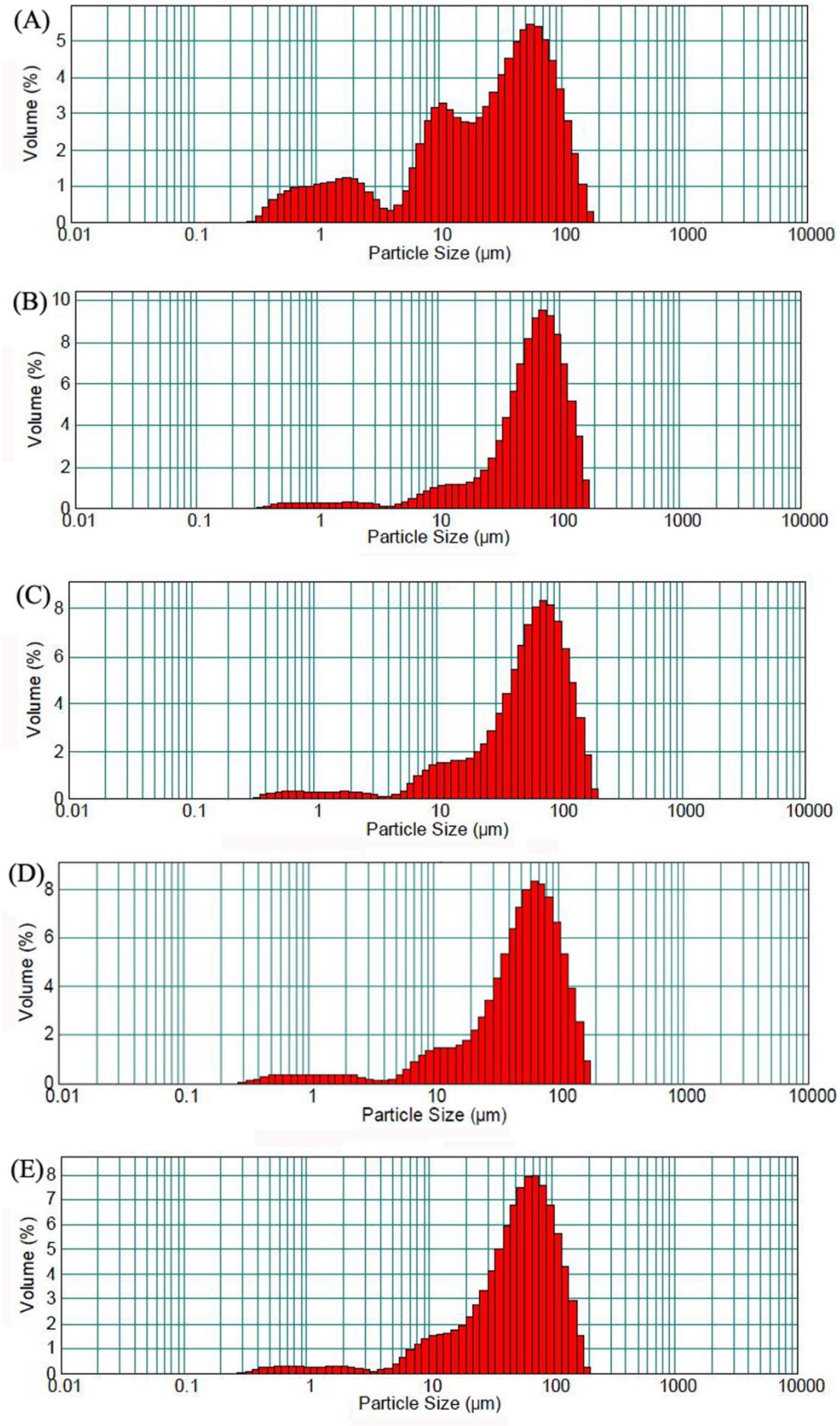

Figure S3. Size distribution of 0Fe-PCCP (A), 1Fe-PCCP (B), 2Fe-PCCP (C), 5Fe-PCCP (D), 10Fe-PCCP (E) powders.

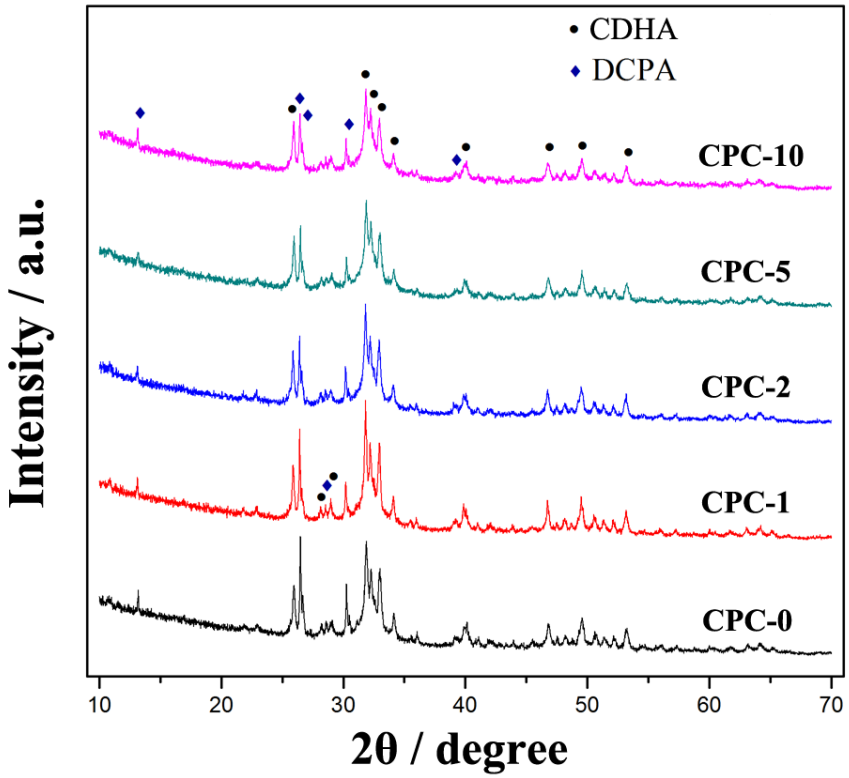

Figure S4. XRD patterns of Fe-CPC samples after they were hydrated for 3 days

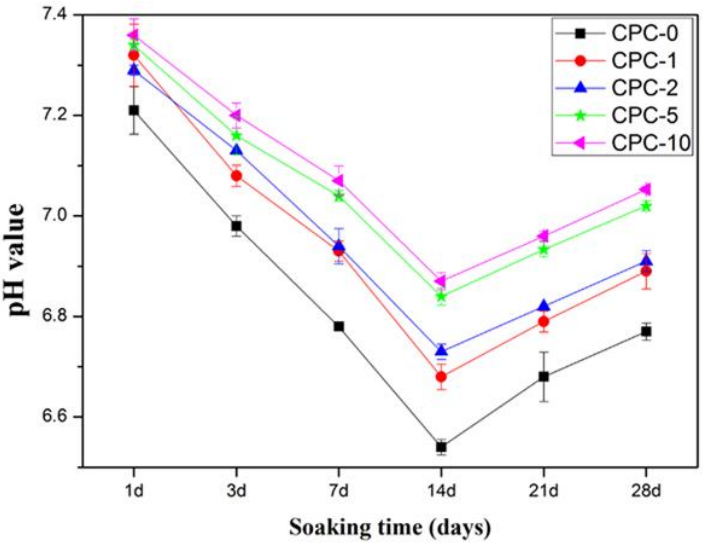

Figure S5. pH values of the collected PBS at each time point.

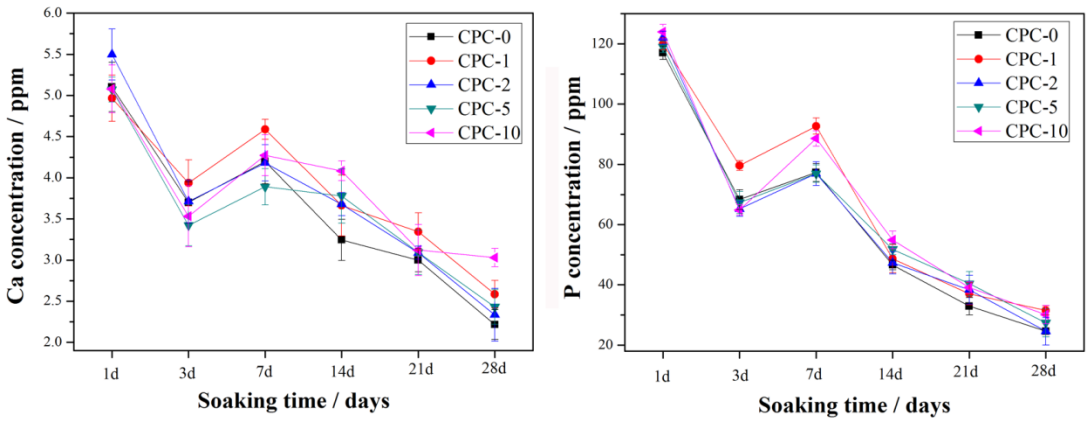

Figure S6. The concentrations of Ca and P in the collected PBS at each time point.

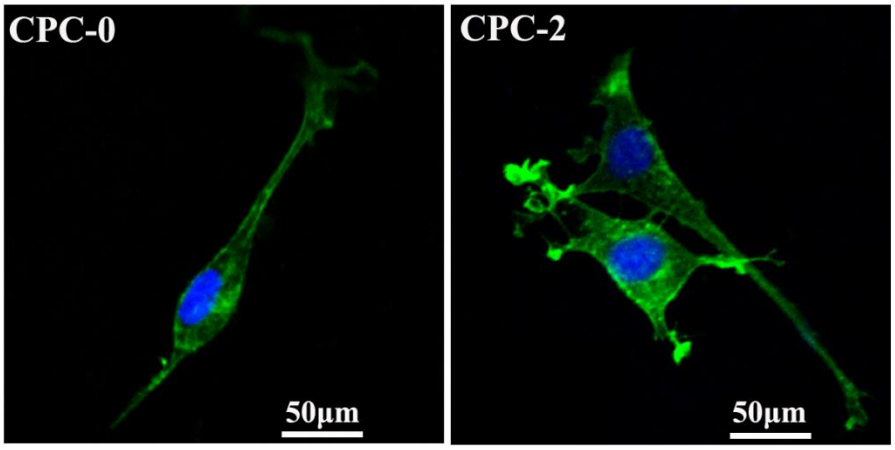

Figure S7. Fluorescence photographs of cytoskeleton organization and nucleus of mBMSCs seeded on CPC-0 and CPC-2 for 24 hours.

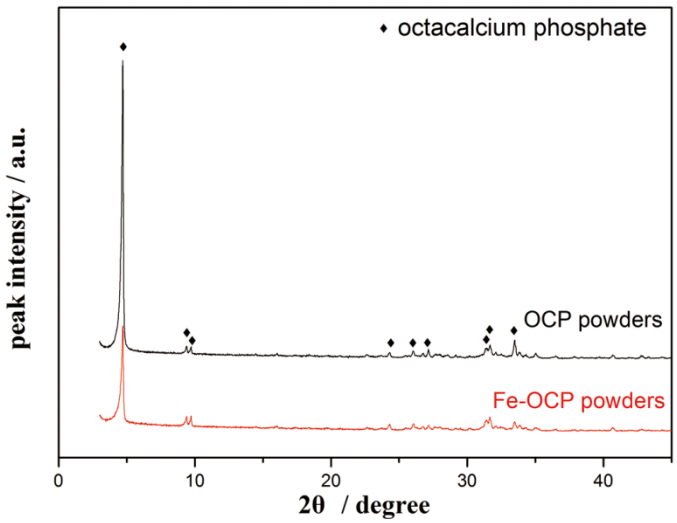

Figure S8. XRD patterns of the synthesized OCP and Fe-OCP powders. Both of the patterns revealed octacalcium phosphate phase, and there was no secondary phase in OCP and Fe-OCP powders. Fe-OCP powders showed lower peak intensity compared with OCP powders due to the substitution of Fe^{3+}.

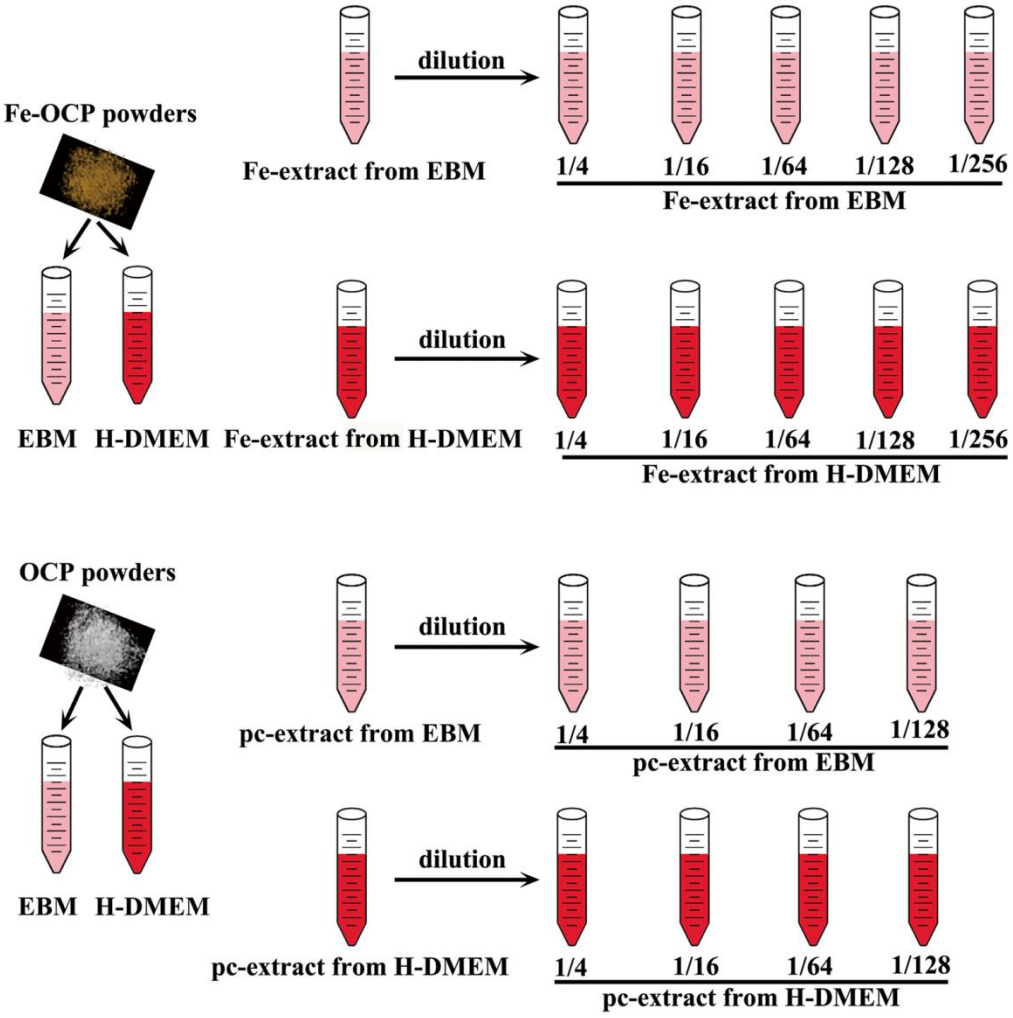

Figure S9. The preparation of a series of Fe-extracts and pc-extracts. In the ALP, RT-PCR and ARS experiments of rMSCs, sodium β-glycerophosphate, dexamethasone and vitamin C were added into extracts with final concentrations of 10 mM, 10 nM and 50 mg/mL respectively.

Table S1. Lattice parameters of Fe-PCCP

	0Fe-PCCP	1Fe-PCCP	2Fe-PCCP	5Fe-PCCP	10Fe-PCCP
a axis	9.40618	9.40776	9.40764	9.40791	9.41108
c axis	6.88541	6.88276	6.88270	6.88145	6.88148

Table S2. Atomic contents and ratios of Ca, P and Fe in Fe-PCCP resulting from XRF analysis

	Ca/mol	P/mol	Fe/mol	Fe/(Fe+Ca)	(Ca+Fe)/P
0Fe-PCCP	0.61839	0.44225	0.00062	0.00101	1.39969
1Fe-PCCP	0.62196	0.43972	0.00688	0.01093	1.43010
2Fe-PCCP	0.60804	0.42704	0.01350	0.02172	1.45544
5Fe-PCCP	0.47768	0.33718	0.02488	0.04949	1.49045
10Fe-PCCP	0.43875	0.32366	0.04900	0.10046	1.50697

Table S3. Primers used for RT-PCR analysis

Target gene	Forward primer sequence (5′-3′)	Reverse primer sequence (5′-3′)
GAPDH [1]	TGTGTCCGTCGTGGATCTGA	TTGCTGTTGAAGTCGCAGGAG
Collagen-I	ATGCCGCGACCTCAAGATG	TGAGGCACAGACGGCTGAGTA
OC	AGCAGCTTGGCCCAGACCTA	TAGCGCCGGAGTCTGTTCACTAC
OPN	TGCAAACACCGTTGTAACCAAAAGC	TGCAGTGGCCGTTTGCATTTCT
Runx-2	CACTGGCGGTGCAACAAGA	TTTCATAACAGCGGAGGCATTTC
GAPDH [2]	AGAAAAACCTGCCAAATATGATGAC	TGGGTGTCGCTGTTGAAGTC
VEGF	TGCGGATCAAACCTCACCA	CAGGGATTTTTCTTGTCTTGCT
eNOS	TGTCCAACATGCTGCTGGAAATTG	AGGAGGTCTTCTTCCTGGTGATGCC

Note: [1] Primer used for rMSCs. [2] Primer used for HUVECs.